

# Delivered Image Quality Budget for the Discovery Channel Telescope

Byron Smith\*<sup>a</sup>, Anastacia Manuel<sup>b</sup>

<sup>a</sup>Lowell Observatory, 1400 W. Mars Hill Road, Flagstaff, AZ 86001;

<sup>b</sup>University of Arizona College of Optical Sciences, 1630 E. University Blvd., Tucson, AZ 85721

## ABSTRACT

The Discovery Channel Telescope (DCT) is a 4.3-meter telescope designed for dual optical configurations, featuring an  $f/6.1$ ,  $0.5^\circ$  FoV, Ritchey-Chretien prescription, and a corrected  $f/2.3$ ,  $2^\circ$  FoV, prime focus. The DCT is expected to typically deliver sub-arcsecond images, with a telescope and local seeing contribution of  $<0.28''$  FWHM at the R-C focus and  $<0.38''$  FWHM at the prime focus. The Delivered Image Quality (DIQ) budget considers errors from design residuals, manufacturing, environmental effects, and control system limitations. We present an overview of the analytical methods used, including sensitivity analysis for determining collimation effects, and a summary of contributors to the overall system performance.

**Keywords:** DCT, Lowell Observatory, image quality, error budget, sensitivity analysis

## 1. INTRODUCTION

The delivered image quality (DIQ) budget is a systems engineering tool to flow down requirements and account for degradation sources to ensure the top-level image quality requirement is met. This paper describes the development of the delivered image quality budget for a 4-meter class optical telescope designed to deliver seeing limited images. The intent of the authors is to provide a guide to a development approach and reasonable allocation values for others who may be embarking on similar projects, as earlier budgets were useful to the DCT project, particularly during the conceptual design phase. To this end, we present a discussion of the image quality requirements, description of the analytical approach, particulars of the contributing terms, a summary of the budget values, and some recommendations for future efforts.

The prime focus design (shown on the left in Figure 1) includes the primary mirror with a prime focus corrector that includes five lenses, a filter and a vacuum window. To compensate for atmospheric diffraction at different pointing angles, the configurations vary in the focus of the corrector assembly and in the decenter in  $y$  and tilt in  $x$  of lens 4. The sensitivities to alignment were calculated using the zenith pointing configuration. The Ritchey-Chretien design includes the primary and secondary mirrors, along with some other elements (ADC, fold mirror, etc.) as shown in Figure 1 on the right.

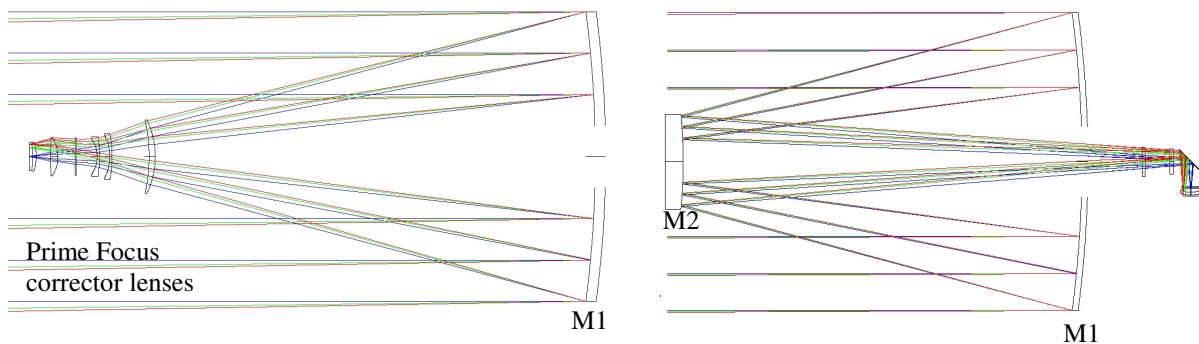


Figure 1. Left: Optical model of DCT prime focus configuration. Fields shown are  $0^\circ$  (blue),  $0.7^\circ$  (green), and  $1^\circ$  (red).  
Right: Optical model of DCT RC configuration. Fields shown are  $0^\circ$  (blue),  $0.175^\circ$  (green), and  $0.25^\circ$  (red).

\* [bsmith@lowell.edu](mailto:bsmith@lowell.edu); phone: 928-233-3258; fax: 928-233-3268; lowell.edu

## 2. REQUIREMENTS

The DCT is designed to be a general purpose research telescope, designed to accommodate the needs of the Lowell Observatory, both present and future. As such, it is a particularly flexible telescope, with provisions for substantial instrumentation at the prime, Cassegrain, Nasmyth, and bent-Cassegrain focal stations, relatively wide fields-of-view, and broad spectral bandpasses. The telescope is designed to deliver seeing limiting images, and although it is anticipated that the DCT will likely eventually support adaptive optics, AO is considered out of the present scope and not specifically addressed.

The top-level performance requirements are specified separately for the prime and Cassegrain focal stations, in terms of degradation of the atmospheric seeing as measured during the site testing campaign, summarized in Figure 2<sup>1</sup>. The f/6.1 Cassegrain specification is a <10% degradation of the 1st quartile seeing, or 0.28" FWHM, across the 0.5° field of view. Based upon results of the conceptual design studies, the requirement was relaxed to a <10% degradation of the median seeing, or 0.38" FWHM, for the much wider and faster prime focus configuration (f/2.3 across a 2° field of view). These requirements cover both the telescope and local seeing contributions.

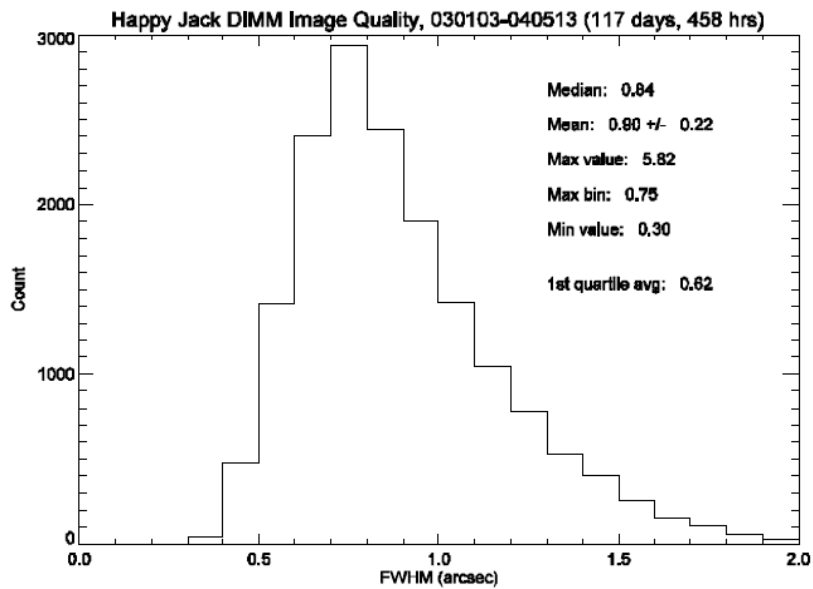


Figure 2. Histogram of DIMM measured atmospheric seeing at Happy Jack site.

The above specifications assume that the guiding and wave front sensing loops are closed. To guarantee a minimum level of performance in the event a guide or wave front sensing star is unavailable, a relaxed specification of 0.47" FWHM is made for the open-loop case, sufficient to return one arc-second images with median atmospheric seeing.

The image quality requirements are specified to apply for the Johnson (U,B,V,R,&I) filter bands and a broad bandpass spanning B+V+R.

As the delivered image quality is based on a proportional degradation of the atmospheric seeing, it is relaxed as a function of zenith distance. The relaxation is specified to be  $\sec(z)^{0.6}$ , approximating the observed increase in atmospheric seeing. If the telescope is assumed to be aligned at Zenith, a single specification at  $z=30^\circ$  (or vice versa) would constrain the performance well and simplify the analysis somewhat.

### 3. ANALYTICAL APPROACH

This section describes the analytical framework for the development of the image quality budget. General accounting assumptions are covered, as in the optical sensitivity analysis which is the basis for many of individual contribution calculations.

#### 3.1. General Assumptions

The DCT image quality budget follows the standard accounting approach. Unless otherwise specified, contributions are assumed to be uncorrelated and normally distributed. As such, they are combined by the root sum square (RSS) method.

The units used herein for contributions are generally arc-seconds at full-width half-maximum (FWHM). This being the standard unit for astronomical image sizes which are necessarily measured in the presence of background noise (precluding an accurate RMS calculation). For analytical convenience it would be reasonable to develop the budget in terms of engineering units (e.g.  $\mu$ radians RMS), converting only once to arc-seconds FWHM for the final result. The decision is predominantly a matter of preference. Whichever system is selected, it is recommended to explicitly denote RMS vs. FWHM on all relevant quantities; otherwise confusion between the two is invited (as observed in more than one error budget).

For convenience, equivalent measures of Gaussian irradiance profiles are listed below:

- 0.425 1D RMS radius ( $\sigma$  for Gaussian profile)
- 0.601 2D RMS radius ( $\sqrt{2}$ \* 1D radius)
- 1.000 FWHM
- 1.000 50% encircled energy diameter (50%EE)
- 1.201 1-e<sup>-1</sup> encircled energy diameter (63%EE)
- 1.524 80% encircled energy diameter (80%EE)

#### 3.2. Optical Alignment Sensitivities

The sensitivities to element misalignments for both the prime focus and Ritchey-Chretien designs shown in Figure 1 were determined using a lens design program. The sensitivities are defined as the change in performance criteria  $\Delta\Phi$  divided by the amount of a small perturbation  $\Delta x$ :

$$\text{Sensitivity} = \Delta\Phi/\Delta x.$$

An inverse limit sensitivity analysis was used in the lens design program to find the perturbation sizes  $\Delta x$  such that the RMS spot size increased by 10%. (This was to ensure the perturbation was large enough to cause an effect, but not so large that the effect became nonlinear.)

#### 3.3. RMS spot size sensitivities

The figure of merit ( $\Phi$ ) in the first sensitivity analysis is RMS spot size. The RMS spot size figure of merit is a single number that is averaged over twelve points throughout the field and ten wavelengths (ranging from 0.3 to 1.1  $\mu$ m). The sensitivities can be used to estimate the size of the spot of a misaligned system by adding in quadrature the sensitivity\*misalignment for all the element perturbations and the nominal value of the aligned system (listed in following table). (The effects are added in quadrature because they are assumed to be uncorrelated.) Similarly, the pointing sensitivities can be used to estimate the pointing error of a misaligned system by adding in quadrature the sensitivity\*misalignment for all the element perturbations (there is no pointing error for the aligned system).

The nominal spot sizes for the aligned systems are as shown in Table 1.

Table 1. Nominal spot sizes for the aligned DCT models.

System	RMS spot radius in mm	FWHM spot size in mm (mult. by 1.6)	FWHM spot size in arc-seconds (mult. by scale factor)
Prime Focus	0.00474	0.008	0.161
Ritchey-Chretien	0.00604	0.010	0.077
Ritchey-Chretien (re-opt with focus compensator)	0.00598	0.010	0.076

To find the scale factor to change from FWHM in mm to arc-sec, divide 206265 arc-sec/radians by the effective focal length in mm. Due to the different effective focal lengths, each configuration has a different scale factor, as listed in Table 2.

Table 2. Scale factors for the two DCT configurations.

	Effective Focal Length (mm)	Scale Factor (arcsec/mm)
Prime Focus Design	9742.91	21.171
RC Design	25959.7	7.946

As an example, if the primary mirror is decentered in y by  $\Delta x = 0.00973\text{mm}$  in the prime focus model, the RMS spot size figure of merit increases from 0.00474mm to 0.00521mm. This increase (found by root difference squared) is  $\Delta\Phi = 0.00217\text{mm}$ . Therefore, the sensitivity for RMS spot size is:

$$\Delta\Phi/\Delta x = 0.00217\text{mm}/0.00973\text{mm} = 0.223\text{mm/mm}$$

To convert to FWHM spot size in mm, this value is multiplied by 1.6 and then multiplied by 21.2 to convert to arc-seconds. The final sensitivity (listed in Table 3) is thus 7.56 arc-sec/mm.

### 3.4. Pointing sensitivities

The second group of sensitivities found was for pointing errors that resulted for the same perturbations that gave a 10% increase in RMS spot size. The pointing error recorded was the centroid position in mm for the on-axis field.

### 3.5. Results

For each set of sensitivities (spot size and pointing), two different cases of compensators were investigated. The compensators are the degrees of freedom allowed to vary during the optimization procedure corresponding to the actual degrees of freedom used for correction of the system in operation. The first case investigated had no compensators; the second case used the axial position of the secondary mirror (RC configuration) or the prime focus corrector relative to the primary mirror (Prime focus configuration).

Table 3. Spot size and pointing sensitivities for two different DCT configurations. The sensitivities are in units of arc-sec/mm, except for the tilt motions, which are arc-sec/deg.

Prime Focus Design						
i	Element	Motion	Sensitivity to FWHM Spot Size		Pointing Error Sensitivity	
			no comp	with comp	no comp	with comp
1	PM to group of lenses	Focus	7.56		0.00	
2	Primary Mirror	Decenter in y	0.61	0.61	25.26	25.26
3	Primary Mirror	Tilt in x	82.59	82.58	7129.67	7129.67

4	Group of lenses incl FP	Decenter in y	0.61	0.61	25.26	25.26
5	Group of lenses incl FP	Tilt in x	16.05	16.05	708.23	708.23
<b>Ritchey- Chretien Design</b>						
i	Element	Motion	Sensitivity to FWHM Spot Size		Pointing Error Sensitivity	
			no comp	with comp	no comp	with comp
1	PM to SM	Focus	11.31		0.00	0.00
2	Primary Mirror	Decenter in y	0.59	0.59	25.26	25.26
3	Primary Mirror	Tilt in x	78.37	78.37	7129.12	7129.12
4	SM to E1 Spacing	Focus	0.55	0.02	0.00	0.00
	Secondary Mirror Position	Focus	12.33		0.00	0.00
5	Secondary Mirror	Decenter in y	0.59	0.59	-17.20	-17.20
6	Secondary Mirror	Tilt in x	21.28	21.28	-2123.81	-2123.81
7	E1 to ADC Spacing	Focus	0.58	0.02	0.00	0.00
	E1 Position	Focus	0.06	0.00	0.00	0.00
8	Element 1	Decenter in y	0.01	0.01	0.23	0.23
9	Element 1	Tilt in x	0.11	0.11	-2.24	-2.09
10	FM to guide probe	Focus	1.08	0.00	0.00	0.00
	Fold Mirror Position	Focus	1.17	0.04	0.00	0.00
11	Fold Mirror	Decenter in y	0.00	0.00	0.00	0.00
12	Fold Mirror	Tilt in x	1.39	1.39	134.28	134.28
13	E2/Window to focus Spacing	Focus	0.99	0.00	0.00	0.00
	E2 Position	Focus	0.43	0.01	0.00	0.00
14	Element 2/Window	Decenter in y	0.02	0.02	-0.34	-0.34
15	Element 2/Window	Tilt in x	0.14	0.14	1.81	1.81
16	Focal Plane	Tilt in x	0.72	0.72	0.00	0.00

Depending on how the mechanical degrees of freedom are defined when an optical system is assembled, one might be interested in sensitivities of either the spacings or the positions of the elements. For this reason, both sets of sensitivities are included in the table above. When a spacing sensitivity is found, the axial thickness between elements is perturbed and as a result, the total length of the system is changed by the same amount. When a sensitivity on a position is found, the position of the element is perturbed within the space that it resides in and the total length of the system is unchanged. In this analysis, to find position sensitivities, the space before the element is increased and a pickup decreases the space after the element by the same amount.

For the table above (Table 3), only the M2 spacing is considered for the RC compensation. The sensitivities were only reduced for the focus degrees of freedom. However, M2 gravity-induced decenter will be compensated with tilt. The following table (Table 4) compares the perturbations for Secondary mirror decenter in y degree of freedom for the case of no compensation and with tilt compensation. Table 4 lists the FWHM spot size sensitivity of M2 to decenter in y motions compensated by M2 tilt in x.

Table 4. FWHM spot size sensitivity of M2.

i	Element	Motion	Sensitivity to FWHM Spot Size	
			no comp	with tilt comp
5	Secondary Mirror	Decenter in y	0.586	0.100

Tilting M2 is an effective compensator for M2 gravity-induced decenter because the sensitivity is about 1/6 as large.

## **4. BUDGET TERMS**

The section provides details on the individual terms contributing to the image quality budget. The budget terms are categorized according to their cause: limitations of the basic optical design, errors in implementing that design, environmental effects (gravity, thermal, wind, and seeing), or performance limitations of major supporting systems (active optics and mount). Definitions are provided for what effects are included in each term, along with a description of how the term was quantified, and some representative values provided. The following section provides a more detailed summary of the individual image size contributions.

### **4.1. Optical Design**

The optical design contributions are divided into three sections: design residual, diffraction, and dispersion.

#### **4.1.1. Design Residual**

The design residual captures the limiting performance of the telescope and refractive correctors, based on a geometrical optics analysis. The conceptual design effort for the DCT included the development of corrector prescriptions for the RC and prime foci<sup>2,3</sup>. These reference designs were then used as the basis of allocations for corrector design residuals in the DIQ budget. The analysis was based on ray-tracing of the ideal collimation condition to develop an average of spot-sizes across the fields of view, as described in the sensitivity analysis section, above.

#### **4.1.2. Diffraction**

The diffractive contribution of the telescope aperture was analyzed, considering the effects of the central obscuration and spider. The approach was based on a simple calculation of fractional encircled energy due to the diffraction around the masking elements (circles and rectangles), without the computation of a detailed point spread function<sup>4</sup>. Since the intensity distribution of the diffraction pattern is non-gaussian, with comparatively more energy outside of the FWHM diameter, the 50% encircled energy diameter is used as the measure of the contribution to image degradation.

#### **4.1.3. Dispersion**

Dispersion is considered as the effect of differential atmospheric refraction across the observing band pass, and is a function of zenith distance, wavelength, and bandwidth of observation. The differential refraction is large, particularly across the broad bandpass filter, and must be corrected. An atmospheric dispersion corrector (ADC) was included in the prime focus corrector design effort, resulting in a simple yet very effective design (see Figure 3). An allocation of half the prime focus ADC residual was made for the slower and more narrow field of view RC beam.

$$\theta_{\text{spec}}(z) := 0.28 \cdot \text{arcsec} \cdot \cos(z)^{-0.6}$$

$$\theta_{\text{ADC}}(z) := 0.05 \cdot \text{arcsec} \cdot (\sec(z) - 1)$$

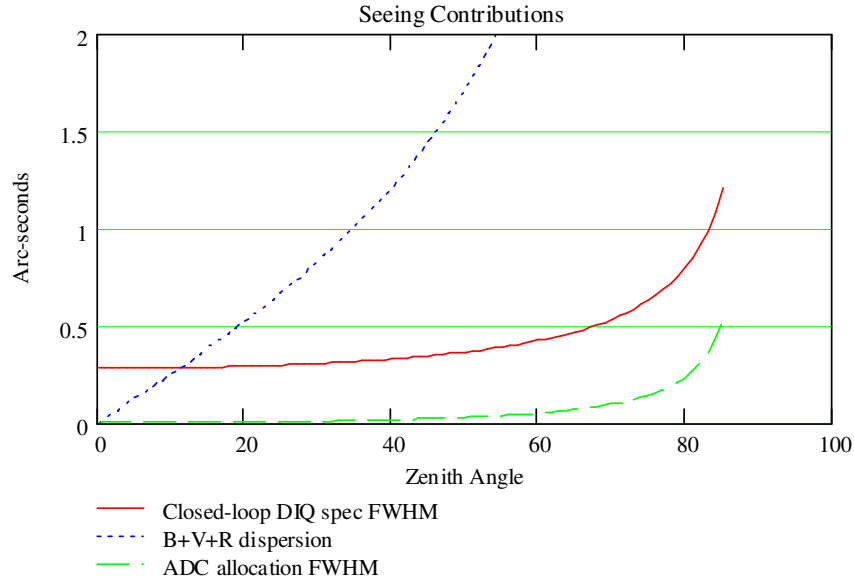


Figure 3. Performance of the prime focus ADC and uncorrected dispersion.

## 4.2. Fabrication and Assembly

The fabrication and assembly section covers fabrication (figuring) of the optical surfaces and alignment of the elements within groups. Alignment errors between groups are covered in the static alignment section, below.

### 4.2.1. Fabrication

The primary mirror figure is specified in terms of tolerances on the vertex radius of curvature, conic constant, and a wavefront structure function defined to have a Kolmogorov spectrum.<sup>5</sup> The radius and conic tolerances are specified to be  $\pm 10\text{mm}$  and  $\pm 0.0002$ , respectively, although the radius was required to be measured to  $< 1\text{mm}$ , and the system prescription revisited based on the as-built radius. Fabrication sensitivities were determined in a manner similar to the alignment sensitivity analysis, allowing focus compensation, and used to determine the image size contribution. The structure function is described by parameters  $r_0=125\text{cm}$  and  $\lambda=500\text{nm}$ , giving a FWHM image size contribution of  $0.98 \cdot \lambda / r_0 = 0.081''$  FWHM.

A structure function is used because large aspheric optics are generally figured with relatively small tools, and it is important to constrain the spatial derivatives (slopes) as well as the phase errors. A Kolmogorov spectrum is one reasonable way to define such a structure function, but while similar to atmospheric phase errors it bears little resemblance to typical figuring errors. In practice the mid-spatial frequencies (comparable to tool size) will be the most challenging portion of the structure function, as seen below. For a seeing limited telescope, a simple requirement (e.g. encircled energy size) would also reasonably constrain the slope errors (see Figure 4).

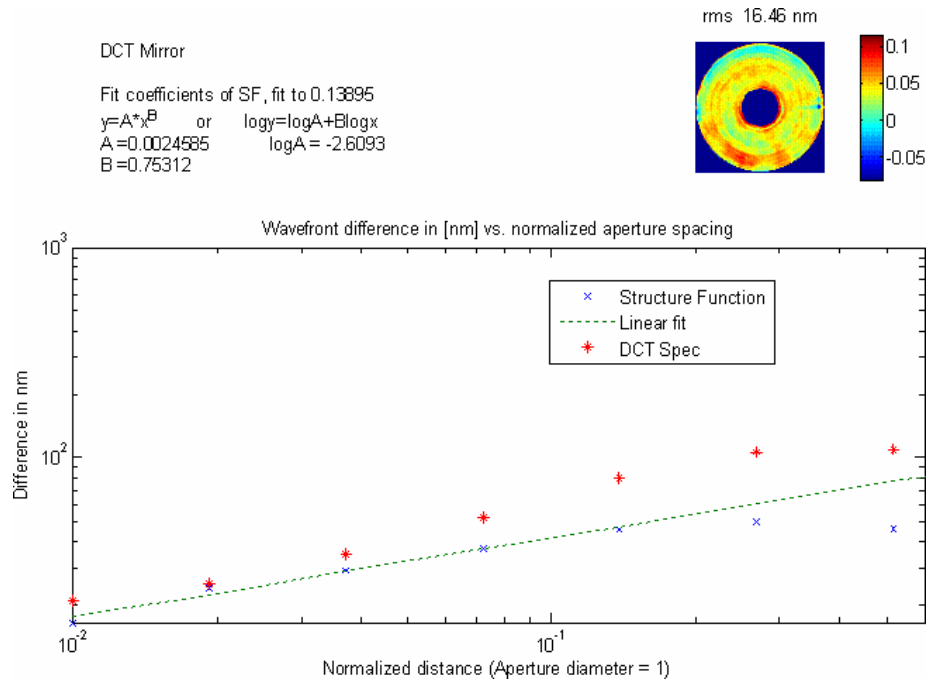


Figure 4. M1 structure function versus requirement.

The secondary mirror figure is similarly specified with radius and conic tolerances of  $\pm 0.5\text{mm}$  and  $\pm 0.0002$ , and a structure function with  $r_0=80\text{cm}$  and  $\lambda=500\text{nm}$ . The image size contribution considers the effect of demagnification ( $m=3.2$ ), yielding a value of  $0.045''$  FWHM.

The refractive corrector optics are specified as  $\lambda/20$  RMS wavefront error per surface, at  $\lambda=633\text{nm}$ . These are assumed to be conventionally figured (with relatively large tools), with the FWHM image size contribution estimated as  $4*\sigma/D$  per surface, where  $\sigma$  is the RMS wavefront error and  $D$  is the 4.3 meter pupil diameter.

#### 4.2.2. Assembly

The RC configuration utilizes a two element corrector, but these are treated as separate groups as early concept designs supported the elements independently. As such, these alignment terms are addressed below.

The prime focus corrector is treated as a seven element group. An assembly tolerance analysis was included as part of the conceptual design effort, resulting in an allocation of  $0.035''$  FWHM within the group.

### 4.3. Static Alignment

Static alignment errors are those introduced during installation and manual alignment. Alignment errors due to environmental effects and limitations of the active optics system (including M1 & M2 tip/tilt/piston) are addressed below.

The DCT optical alignment procedure is primarily based on laser tracker metrology. A single setup on the elevation ring allows visibility of critical datum features, avoiding stitching errors between set ups. In particular, this allows a “snapshot” of element locations to be taken quickly, minimizing thermal drift errors. As such, the measurement accuracies expected for datum features are approximately  $50\mu\text{m}$  RMS. Optical axes of the elements are determined relative to substrate datums in the optical shop during figuring, as this can be done more accurately than at the site with a laser tracker. Installation tolerances were developed as a balance between ease of achievement versus performance sensitivity.

For the purpose of this analysis, the basis of the optical coordinate system is defined as the primary mirror optical axis. That is, the M1 installation error is zero, and all other elements up to and including the focal plane are calculated relative to it. The calculation for each element considers a chain of errors; including M1 axis to substrate, M1 substrate location measurement, element substrate location measurement, location adjustment tolerance, element substrate to axis, and effects of optical folds as necessary. The image size contributions are then calculated using the alignment sensitivities. The expected installation tolerances and image size contributions for the RC system are summarized below in Table 5.

Table 5. RC configuration alignment requirements summary.

Parameter	Max. Permissible Value	Units
M1 Vertex spacing from rotator	$\pm 50$	$\mu\text{m}$
M1 Vertex decenter relative to rotator axis	141	$\mu\text{m}$
M1 Optical axis misalignment with rotator axis	18	$\mu\text{rad}$
M2 Tilt	177	$\mu\text{rad}$
M2 Decenter relative to M1 axis	196	$\mu\text{m}$
M2 – M1 Despace	$\pm 100$	$\mu\text{m}$
Corrector Tilt	146	$\mu\text{rad}$
Corrector Decenter relative to M1 axis	1040	$\mu\text{m}$
Corrector Despace relative to M1	$\pm 274$	$\mu\text{m}$

#### 4.4. Gravity

Gravity deformations alter the figure and alignment of the optics as the telescope changes pointing between zenith and horizon during operation.

Gravity induced figure errors are the relative deflections between the optical surface as tested on its polishing support during figuring and as supported in the telescope during operation. Both of the large DCT mirrors were tested on supports in their zenith pointing orientations (M1 zenith pointing, and M2 nadir), minimizing figure errors at zenith, where the overall performance specification is tightest. The primary mirror was tested on a passive support, which supported the mirror in the same manner as the active support in the telescope, with the polishing support errors included in the figure specification. The secondary will undergo final figuring and testing on its operational support.

Similarly, gravitational alignment errors are the relative deflections between the optical elements as the telescope points away from the nominal alignment orientation. The DCT is nominally aligned at zenith, minimizing collimation errors in that orientation.

Assuming that the resultant wavefront errors due to the deformations at zenith and horizon are uncorrelated, it is possible to analyze the two cases independently and combine the image quality effects via superposition to simplify the analysis at intermediate orientations.

$$\theta(z) = \sqrt{[\theta_z \cdot (\cos(z) - \cos(z_{nom}))]^2 + \theta_h \cdot (\sin(z) - \sin(z_{nom}))]^2}$$

Where:

$\theta(z)$  = image size contribution due to gravity deformation as function of zenith angle

$z$  = zenith angle

$z_{nom}$  = nominal zenith angle at which element was aligned/figured

$\theta_z$  &  $\theta_h$  = image size contributions due to deformations at zenith and horizon

The optical support structure gravity deformation requirements were developed during the conceptual design phase by iterative FEA and optical analysis to establish a workable compromise between performance and cost. For initial estimates of alignment errors, advantage can be taken of the relation between gravity deflections and resonant frequency. The minimum resonant frequency of the optical support structure is often constrained due to dynamic concerns, bounding the maximum gravity deflections:

$$x_g \leq \frac{g}{\omega_0^2}$$

In practice, not all deflections are associated with the lowest modes and homologous design principles can be used to reduce the relative deflections further so the above relation is only a very conservative starting point. For reference, the DCT gravity errors are dominated by the 1.5mm of M2 decenter as the telescope points to horizon.

Although gravity errors are largely repeatable, the bolted steel support structure is expected to exhibit some hysteresis due local micro-yielding and slip at the bolted connections. For the low hysteresis levels and negligible viscous damping typical of optical structures, the full width of the hysteresis loop may be estimated by relation to the structural damping by:

$$\frac{\Delta x}{x_g} \cong \frac{\pi}{2Q}$$

Where:

$\Delta x$  = full width of hysteresis loop

$x_g$  = peak gravity deflections

$Q$  = quality factor of resonant peak

A common damping value used for analysis of such structures is 2% of critical ( $Q = 25$ ). In practice, much lower inherent damping is often realized. Measured  $Q$  factors for DCT structural resonances are in the 50 to 150 range. Taking  $Q=75$  as a typical value, and assuming the error is either  $\pm\Delta x/2$ , an RMS non-repeatability of 1% is then used for the budget.

## 4.5. Thermal

Temperature changes in the environment induce figure and alignment errors in the optical system. This is due both to bulk temperature changes away from the nominal figuring and alignment temperature (20°C), and temperature gradients within the optical system caused by transient changes (e.g. due to the diurnal cycle).

### 4.5.1. M1

The DCT primary mirror substrate is made of Corning Ultra Low Expansion (ULE) material. Due to limitations in boule size, thirteen boules were fused together to form the 4.3m blank. The ULE material has a specified coefficient of thermal expansion of just  $\pm 30$ ppb/°C, but variations of the CTE between and within boules induce thermal stresses as the bulk temperature changes. The magnitude of the resulting figure changes was estimated by FEA to be 281nm RMS over the 30°C operating temperature range, but correctable by the active support to within 9nm RMS due to the low spatial frequencies involved. The lineal error was scaled to an angular error, by assuming the boule diameter to be the spatial period. The mirror figure versus temperature will be calibrated, but temperature measurement errors (budgeted at 2°C)

will limit open-loop correctability. Because of the low CTE, errors due to the small temperature gradients expected in the thin substrate are negligible.

#### 4.5.2. M2

The secondary mirror substrate is made of GE124 fused quartz material, with a much higher CTE than ULE ( $0.5\text{ppm}/^\circ\text{C}$ ), but excellent homogeneity. Both bulk temperature changes and gradients affect the radius of curvature, but this is highly correctable by refocusing the telescope. For open-loop operation, the bulk temperature effect can be calibrated (as part of the overall system focus), but the expected gradients induce a change in curvature which introduces about  $0.09''$  FWHM of focus error.

#### 4.5.3. Alignment

The alignment errors introduced by bulk temperature changes are highly correctable by refocusing the system, with negligible residuals for closed-loop operation. For open-loop operation, the limiting factor is the temperature measurement error. The support structure is large, and its temperature will inevitably be non-uniform, as shown in Figure 5, so a measurement error of  $0.25^\circ\text{C}$  RMS is allocated, assuming the structure can be sufficiently sampled with temperature probes to approximate an average effective temperature. This image size contribution is still one of the largest terms in the open-loop error budget.

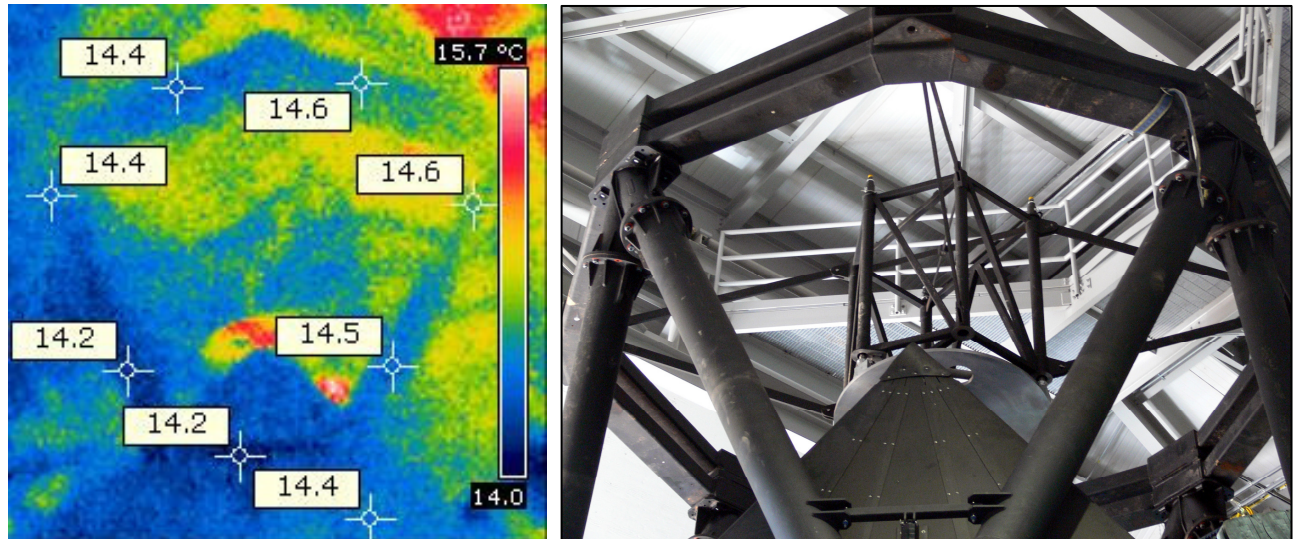


Figure 5. Thermographic (left) and visible (right) images showing temperature variations in OSS structure.

#### 4.6. Wind

The DCT is required to meet its performance specifications with external average wind speeds up to  $10\text{m/s}$ , so the wind deformation analyses are carried out with that assumption. This is conservative, as it is mutually exclusive of the low wind speed ( $2\text{m/s}$ ) condition assumed for the local seeing analyses, below.

For a given external wind speed, the internal velocities are attenuated somewhat by the enclosure. CFD analysis of the DCT enclosure returned results similar to those reported by others.<sup>6</sup> Although the flow details are dependent on incident angle, vent door position, etc., a very simplified profile was used for the basis of deflection analyses assuming a minimum of  $2.5\text{m/s}$  at the center of the dome, increasing radially to  $5\text{m/s}$  at the outer diameter.

For all analyses below, the flow *geometry* is considered steady. However, a simple examination of member sizes and Strouhal numbers suggests that vortex shedding at some orientations and wind speeds is inevitable, possibly coinciding with structural resonances at the higher wind speeds. This is consistent with typical experience reported at existing facilities, and difficult to optimize against given the broad parameter space involved. Windshake effects are then omitted from this budget, and problematic operating conditions will be addressed on a case-by-case basis with aerodynamic treatments or adjustments to ventilation doors as operational experience is accrued.

**4.6.1. M1 and M2**

Deformations of the mirror surfaces on their supports were analyzed by FEA, considering spatial variations in the wind pressure. Power spectra estimates were developed following the methods presented by Harris and Crede.<sup>7</sup> The thin primary mirror benefits greatly from the stiff support and the lightweight structured secondary is inherently stiff, so that wind induced surface errors are small.

**4.6.2. Alignment**

Wind pressure also introduces alignment errors between the optical elements, degrading the image quality. The effect may be divided into two contributions: those due to the spot size increase due to deflections caused by the steady component of the wind, and those due to image motion caused by turbulence in the wind. In both cases, the image degradation is dominated by M2 motion, for which the allowable static deflections are summarized in Table 6.

Table 6. Allowable static M2 wind deflections.

Despace	0.5 $\mu$ m
Decenter	1.0 $\mu$ m
Tilt	0.1" (0.5 $\mu$ rad)

The spot size increase due to the steady component is straightforwardly estimated from FEA of the element displacements, in response to the above described wind pressure distribution on the structure, using the optical alignment sensitivities for spot sizes.

Quantifying the image motion contribution due to turbulence requires some estimate of the wind power spectrum. The PSD used for the DCT analysis is based on a Von Karman velocity spectrum modified by aerodynamic and mechanical admittances.<sup>7</sup> These admittances account for the aerodynamic averaging effect due to the extended size of the structure, and mechanical resonance of the structure, for which a Q of 75 was used, as per the hysteresis estimate in the gravity deformation section above. As the wind pressure is related to the square of the velocity, the pressure power is approximately four times that of the velocity power (neglecting higher order terms). Integrating this power spectrum yields a standard deviation of 22% of the mean pressure. The RMS image motion is then calculated as this fraction of the steady pointing change, using the element displacements and optical alignment sensitivities for pointing. For reference, Figure 6 shows measured windshake spectra from DCT. The structural resonances are clearly visible, with the lowest mount mode (6.4Hz) containing most of the total power.

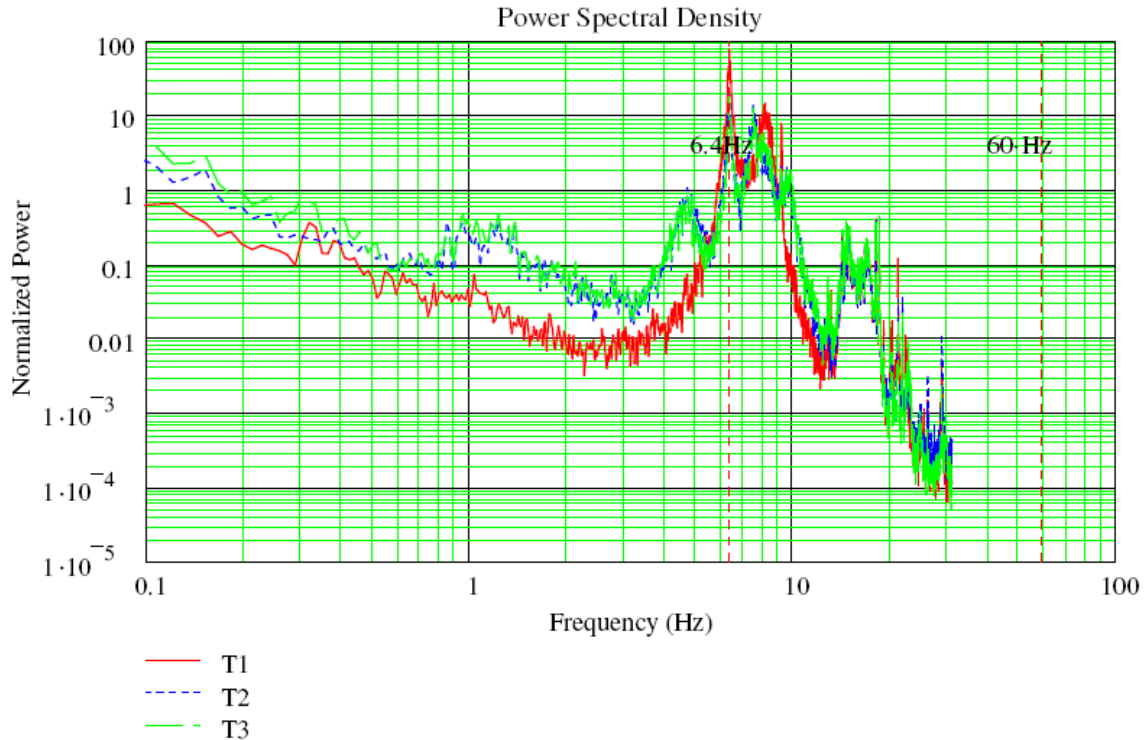


Figure 6. PSD of forces measured on M1 supports showing structural excitation by wind.

#### 4.6.3. Pointing

The wind also induces image motion due to deflection of the mount structure, foundation, and soil. These were estimated following a similar approach to the above, estimating a static deflection by FEA and determining the RMS response to the wind PSD. The mount and foundation deflections were analyzed separately from the building and soil. As the deflections are likely correlated to some degree, these terms are combined linearly in the budget (rather than in quadrature).

### 4.7. Local Seeing

The seeing analysis for the DCT has been presented previously.<sup>8</sup> In general, the analysis considers shell, chamber, mirror, and M2 unit seeing, using empirical relations based on temperature differences or heat flows.<sup>9</sup> One caution is that most of these relations were characterized at large temperature differences producing seeing comparable to atmospheric conditions, and how well they may be extrapolated to small temperature differences is unclear with validation difficult.

#### 4.7.1. Shell Seeing

Shell seeing is considered to be the effect of index variations in the enclosure's external surface boundary layer. In general, radiation to the cold sky cools the surface below ambient, causing thermal (and index) variations in the boundary layer. A thermal model of the facility was utilized to estimate the expected surface temperatures for a variety of different finishes, and empirical relations used to estimate the resulting seeing effects. While low emissivity finishes are desirable, practical considerations such as cost and durability must be considered as well. Ultimately, a self-adhesive aluminum foil finish was selected for the DCT enclosure to minimize shell seeing (0.024" FWHM typical).

#### 4.7.2. Chamber Seeing

Chamber seeing is defined as the effect of index variations within the observing chamber air and the interface between the chamber air volume and exterior. Again, the thermal model of the facility was used to quantify the expected temperature difference between the chamber and exterior, and empirical relations used to estimate the resulting seeing. Given the large diurnal temperature swings at dry high-altitude sites, the thermal mass of the telescope and enclosure will liberate a great deal of heat as the ambient temperature drops over the course of an observing night. For the DCT, typical heats flows are in the tens of kilowatts range, and large ventilation doors are provided to keep the chamber temperature delta and expected seeing small (<0.02" FWHM).

#### 4.7.3. Mirror Seeing

Mirror seeing results from convective heat transfer from the optical surface causing index variations in the optical path. To determine the seeing magnitude and evaluate mitigation strategies, the chamber temperatures computed for the chamber seeing estimate, above, were used for a one dimensional transient conduction analysis of the mirror. Unless encouraged otherwise, the optical surface temperature will lag behind the ambient air resulting in significant seeing. A simple non-contacting cold plate close to the rear surface was found to be effective at minimizing the expected front surface heat transfer with the air and reducing expected seeing (<0.08" FWHM).

#### 4.7.4. M2 Unit Seeing

The M2 unit seeing addresses seeing caused by the thermal plume of the secondary mirror and other equipment in the optical path. The net heat flow from the top-end equipment was estimated, considering transient convection and radiation. The mirror is lightweighted and electrical power dissipation minimized to keep the expected seeing low (<0.07" FWHM).

### 4.8. Active Optics

This section considers the effects of errors within the active optics system on both the figure and alignment of the actively supported mirrors.

#### 4.8.1. M1 Figure

The primary mirror is supported by 120 individually controlled axial actuators, and 36 commonly controlled lateral supports. The axial support forces are controlled around load cells, with parasitic forces limited by flexures and installed tolerances. The lateral supports forces are similarly controlled to maintain the three tangent definers at nominally zero force.

The performance analysis considers both repeatable and non-repeatable errors in every attachment to the mirror, and how correctable the error sources are. In the open-loop case, the repeatable errors are considered calibrated out to the limits of correctability. For closed-loop operation, the non-repeatable terms are considered corrected based on wavefront sensing. The support performance is specified as a function of zenith angle, with the closed loop requirement given below.

$$\theta_{m1} = \sqrt{(0.117" FWHM)^2 + (0.167" FWHM \cdot \sin(z))^2}$$

The reason for this form is that the axial support errors are largely independent of orientation, while the lateral support errors are strongly dependent on the lateral loading.

#### 4.8.2. M2 Figure

The secondary mirror is supported axially within the cell by three passive axial supports and a vacuum regulated to maintain zero force on those supports. Laterally, the mirror is supported by a central hub with a diaphragm flexure. The vacuum system performance is limited by measurement error in the axial support load cells, resulting in very small figure errors (<0.022" FWHM).

#### **4.8.3. M1 Alignment**

To allow for collimation in the prime focus configuration the primary mirror may be articulated in tip, tilt, & piston within its cell. Position feedback is provided by linear gauges at the mirror outer diameter, and adjustments made by commands to the 120 axial supports. The position definition is then highly distributed, so the feedback gauge limits both accuracy and resolution. In the Ritchey-Chretien configuration, the mirror is held to a constant position within the resolution limit of the gauge, which is somewhat better than the overall accuracy. The lateral positioning accuracy is limited by support force errors acting on the compliance of three tangent definers.

During open loop operation, the alignment errors introduce both image motion and spot size errors. Of these, the image motion due to tilt errors is the dominant term ( $\sim 0.07''$  FWHM). In closed loop operation, image motion errors are guided out, and the remaining spot size contributions to image degradation are negligible.

#### **4.8.4. M2 Alignment**

Active collimation of the Ritchey-Chretien configuration is done classically with tip, tilt, & piston control of the secondary mirror and cell assembly. Similar to the primary mirror, position feedback comes from linear gauges, but here the resolution is limited by the three position actuators. Lateral support is entirely passive.

As with the primary mirror, the open loop analysis considers image motion and spot size effects of the accuracy limitations of the support, while closed loop operation assumes image motion to be guided out. Furthermore, with collimation adjusted based on wavefront feedback, the position may be controlled to the resolution limit of the actuators. The open loop contribution of  $0.144''$  FWHM is then reduced considerable under closed-loop operation to  $0.04''$  FWHM.

#### **4.8.5. Wavefront Sensing**

An allocation is made for limitations in the accuracy of the wavefront sensing. The accuracy depends largely on the sensitivity and noise characteristics of the wavefront sensing camera, field of view, bandwidth, and availability requirement. The allocation of  $0.02''$  RMS at a  $0.01\text{Hz}$  bandwidth is readily achievable except for in particularly sparse portions of the sky.

### **4.9. Mount Tracking**

Mount tracking includes the image quality degradations due to the limitations of the gimbal systems (bearings, drives, & encoders).

#### **4.9.1. Drift**

The tracking drift requirement for the DCT is specified separately from the image quality budget, but is  $0.1''$  per minute for open-loop operation. In practice, this is dominated by thermal changes in the mount structure. For closed loop operation, the performance requirement is  $0.1''$  per 10 minutes, largely limited by differential deflection between the guide probe and instrument.

#### **4.9.2. Jitter**

The DCT mount tracking jitter is dominated by periodic errors in the axis encoders. Unfortunately, most of the spectral power is expected above the guide loop bandwidth, and hence uncorrectable. Smaller pointing effects are also contributed by run-out in the axis bearings. The specified mount performance is  $<0.167''$  FWHM of jitter, and analysis suggests half of that may be achievable.

#### **4.9.3. Guiding Accuracy**

As with wavefront sensing, above, an allocation is made for limitations in the guider accuracy. The same tradeoffs apply regarding camera characteristics, field of view, bandwidth, and availability. Similarly, the allocated  $0.02''$  RMS at  $0.1\text{Hz}$  bandwidth is readily achievable over most of the sky.

#### 4.9.4. Misalignment

Run-out in the instrument rotator bearing introduces an alignment error with the instrument to focal plane. These errors are small, and image motion is assumed to be guided out in closed loop operation.

### 5. SUMMARY OF BUDGET TERMS

A summary of error contributions at various zenith angles and optical configurations is provided for reference. These values represent what was reasonably achievable and meeting the performance specifications for the DCT. They should not be considered optimal for any particular project and certainly not the ultimate possible. However, they may well provide a reasonable starting point for others embarking on conceptual designs of similar systems. Figure 7 shows the overall performance for each configuration as a function of zenith angle and compared to the atmospheric seeing. Tables 7, 8, and 9 provide a breakdown for each configuration, at a zenith angle of 30°.

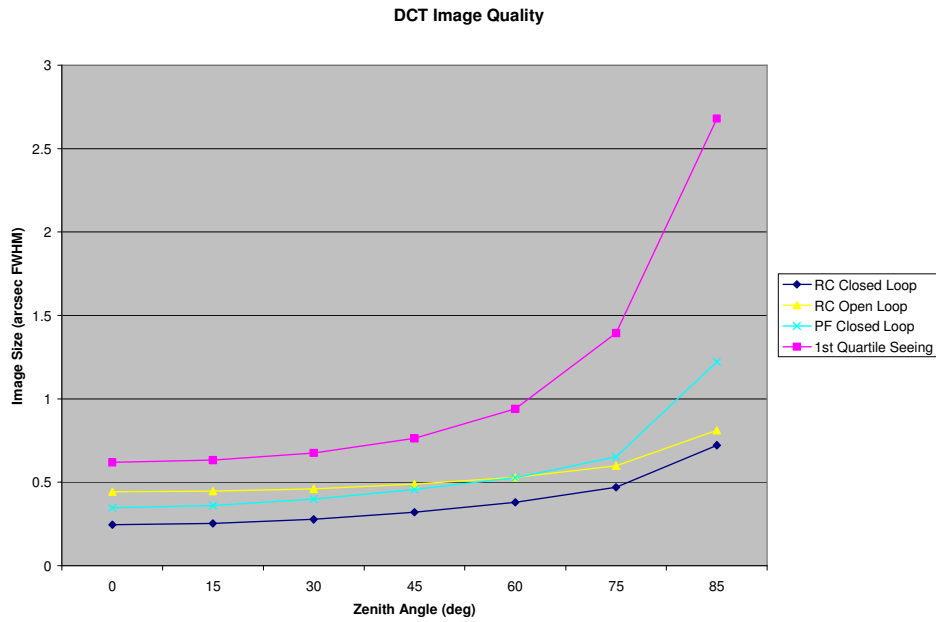


Figure 7. Summary of DCT delivered image quality vs. zenith angle.

Table 7. Breakdown of error budget terms for RC closed-loop configuration at 30° zenith angle.

	Budget Level	0	1	2	3	4
<b>IC Focus DIQ</b>		<b>0.731</b>				
<b>1 Atmosphere</b>		<b>0.676</b>				
1.1 Seeing		0.676				
<b>2 RC Closed Loop</b>		<b>0.278</b>				
2.1 Optical Design		0.106				
2.1.1 Design Residual		0.085				
2.1.2 Diffraction (at $\lambda=1\mu\text{m}$ )		0.063				
2.1.3 Dispersion Residual		0.008				
2.2 Fabrication & Assembly		0.097				
2.2.1 M1		0.084				
2.2.2 M2		0.045				
2.2.3 RC Corrector		0.020				
2.2.4 Mirror Coatings		0.010				
2.3 Static Optical Alignment		0.032				
2.3.1 M1 Alignment		0.000				
2.3.2 M1-M2 Alignment		0.022				
2.3.3 RC Corrector		0.023				
2.4 Gravity Deformations		0.099				
2.4.1 M1 Figure		0.054				
2.4.2 M2 Figure		0.035				
2.4.3 M1-M2-RC Alignment		0.075				
2.5 Thermal Deformations		0.005				
2.5.1 M1 Figure		0.005				
2.5.2 M2 Figure		0.000				
2.5.3 M1-M2-RC Alignment		0.000				
2.6 Wind Deformations		0.061				
2.6.1 M1 Figure		0.033				
2.6.2 M2 Figure		0.002				
2.6.3 M1-M2-RCC Alignment		0.013				
2.6.4 Pointing		0.049				
2.7 Facility-Induced Seeing		0.111				
2.7.1 Shell Seeing		0.024				
2.7.2 Chamber Seeing		0.020				
2.7.3 Primary Mirror Seeing		0.079				
2.7.4 M2 Unit Seeing		0.071				
2.8 Active Optics		0.151				
2.8.1 M1 Support		0.143				
2.8.2 M2 Support		0.022				
2.8.3 M1 Alignment		0.0012				
2.8.4 M2 Alignment		0.039				
2.8.5 Wavefront Sensing		0.01				
2.9 Mount-Induced Image Smear		0.084				
2.9.1 Mount Drift		0.000				
2.9.2 Mount Jitter		0.083				
2.9.3 Misalignment		0.015				
<b>3 RC Instrument and Focal Plane</b>		<b>0.032</b>				
3.1 Detector MTF		0.032				
3.1.1 Detector Non-flatness		0.030				
3.1.2 Detector CTE		0.010				

<b>All Telescope:</b>	<b>0.278</b>
<b>Specification:</b>	<b>0.30524</b>
<b>Margin:</b>	<b>0.1264</b>

Table 8. Breakdown of error budget terms for RC open-loop configuration at 30° zenith angle.

	Budget Level	0	1	2	3	4
<b>RC Focus DIQ</b>		<b>0.820</b>				
<b>1 Atmosphere</b>		<b>0.676</b>				
1.1 Seeing		0.676				
<b>2 RC Telescope</b>		<b>0.462</b>				
2.1 Optical Design		0.106				
2.1.1 Design Residual		0.085				
2.1.2 Diffraction (at $\lambda=1\mu\text{m}$ )		0.063				
2.1.3 Dispersion Residual		0.008				
2.2 Fabrication & Assembly		0.097				
2.2.1 M1		0.084				
2.2.2 M2		0.045				
2.2.3 RC Corrector		0.020				
2.2.4 Mirror Coatings		0.010				
2.3 Static Optical Alignment		0.104				
2.3.1 M1 Alignment		0.000				
2.3.2 M1-M2 Alignment		0.101				
2.3.3 RC Corrector		0.023				
2.4 Gravity Deformations		0.158				
2.4.1 M1 Figure		0.054				
2.4.2 M2 Figure		0.035				
2.4.3 M1-M2-RC Alignment		0.144				
2.5 Thermal Deformations		0.231				
2.5.1 M1 Figure		0.010				
2.5.2 M2 Figure		0.090				
2.5.3 M1-M2-RC Alignment		0.212				
2.6 Wind Deformations		0.061				
2.6.1 M1 Figure		0.033				
2.6.2 M2 Figure		0.002				
2.6.3 M1-M2-RCC Alignment		0.013				
2.6.4 Pointing		0.049				
2.7 Facility-Induced Seeing		0.111				
2.7.1 Shell Seeing		0.024				
2.7.2 Chamber Seeing		0.020				
2.7.3 Primary Mirror Seeing		0.079				
2.7.4 M2 Unit Seeing		0.071				
2.8 Active Optics		0.246				
2.8.1 M1 Support		0.186				
2.8.2 M2 Support		0.022				
2.8.3 M1 Alignment		0.068				
2.8.4 M2 Alignment		0.144				
2.8.5 Wavefront Sensing		0.01				
2.9 Mount-Induced Image Smear		0.167				
2.9.1 Mount Drift		0.000				
2.9.2 Mount Jitter		0.166				
2.9.3 Misalignment		0.015				
<b>3 RC Instrument and Focal Plane</b>		<b>0.032</b>				
3.1 Detector MTF		0.032				
3.1.1 Detector Non-flatness		0.030				
3.1.2 Detector CTE		0.010				

**All Telescope: 0.462**  
**Specification: 0.51237**  
**Margin: 0.22066**

Table 9. Breakdown of error budget terms for prime focus closed-loop configuration at 30° zenith angle.

	Budget Level 0	1	2	3	4
<b>Prime Focus DIQ</b>	<b>1.005</b>				
<b>1 Atmosphere</b>		<b>0.916</b>			
1.1 Seeing			0.916		
<b>2 PF Telescope</b>		<b>0.400</b>			
2.1 Optical Design			0.220		
2.1.1 Design Residual				0.210	
2.1.2 Diffraction (at $\lambda=1\mu\text{m}$ )				0.065	
2.1.3 Dispersion Residual				0.015	
2.2 Fabrication & Assembly			0.121		
2.2.1 M1				0.084	
2.2.2 PFC				0.088	
2.2.3 Mirror Coatings				0.010	
2.3 Static Optical Alignment			0.080		
2.3.1 M1 Alignment				0.000	
2.3.2 PFA Tip/Tilt				0.080	
2.4 Gravity Deformations			0.191		
2.4.1 M1				0.054	
2.4.2 PFA				0.070	
2.4.3 M1-PFA Alignment				0.170	
2.5 Thermal Deformations			0.095		
2.5.1 M1				0.005	
2.5.2 PFA				0.095	
2.5.3 M1-PFA Alignment				0.000	
2.6 Wind Deformations			0.066		
2.6.1 M1				0.033	
2.6.2 M1-PFA Alignment				0.030	
2.6.3 Pointing				0.049	
2.7 Facility-Induced Seeing			0.111		
2.7.1 Shell Seeing				0.024	
2.7.2 Chamber Seeing				0.020	
2.7.3 Primary Mirror Seeing				0.079	
2.7.4 PFA Unit Seeing				0.071	
2.8 Active Optics			0.146		
2.8.1 M1 Support				0.143	
2.8.2 M1 Alignment				0.001	
2.8.2 Wavefront Sensing				0.030	
2.9 Mount-Induced Image Smear			0.083		
2.9.1 Mount Drift				0.000	
2.9.2 Mount Jitter				0.083	
2.9.3 Misalignment				0.000	
<b>3 PF Instrument and Focal Plane</b>		<b>0.100</b>			
3.1 Detector MTF			0.100		
3.1.1 Detector Non-flatness				0.100	
3.1.2 Detector CTE				0.010	

**All Telescope: 0.400**  
**Specification: 0.4142526**  
**Margin: 0.1059127**

## REFERENCES

- [1] Bida, T.A., Dunham, E.W., Bright, L.P. and Corson, C., "Site testing for the Discovery Channel Telescope," Proc. SPIE 5489 (2004).
- [2] MacFarlane, M.J. and Dunham, E.W., "Optical design of the Discovery Channel," Proc. SPIE 5489 (2004).
- [3] MacFarlane, M.J. and Dunham, E.W., "Simplifying the prime focus corrector of the Discovery Channel Telescope," Proc. SPIE 6269-81 (2006).
- [4] Harvey, J.E. James E. Harvey, "Diffraction effects of telescope secondary mirror spiders on various image quality criteria," Applied Optics 34(28), 6337-6349 (Oct 1995).
- [5] Parks, R.E., "Specifications: figure and finish are not enough," Proc. SPIE 7071 (2008).
- [6] Cho, M.K., Stepp, L.M. and Kim, S., "Wind buffeting effects on the Gemini 8-m primary mirrors," Proc. SPIE 4444, 302 (2001).
- [7] Harris, C. M. and Crede, C.E., [Shock and Vibration Handbook, 2nd Ed.], McGraw-Hill, New York, (1976).
- [8] Blanco, D., "Estimating local seeing at the DCT facility," Proc. SPIE 7012-3V (2008).
- [9] Zago, L., "Engineering handbook for local and dome seeing," Proc. SPIE 2871, 726, (1997).